A Hall-Effect Thruster Plume and Spacecraft Interactions Modeling Package [*†]

I.G. Mikellides, G.A. Jongeward, G.A., B.M. Gardner, I. Katz[‡], M.J. Mandell and V.A. Davis
Science Applications International Corporation
9455 Towne Center Drive, MS W2076
San Diego, CA 92121
Ph: (858) 826-1649
Ioannis.G.Mikellides@saic.com

IEPC-01-251

A comprehensive modeling package for determining Hall-effect thruster (HET) plume interactions with spacecraft systems is presented. The package combines three different computer tools: a 1-D HET algorithm to provide plasma conditions near the thruster exit, a 2-D plume code to produce a map of the exhaust, and an enhanced version of the Environment Work Bench (EWB) to assess spacecraft surface interactions with plumes, in 3-D. The 1-D algorithm accounts for a variety of physical processes pertinent to Hall thrusters and includes a phenomenological model for wall effects. The plume map is generated using a 2-D code that computes the expansion of the main beam using a fluid algorithm. Resonant charge-exchange is determined using a Particle-in-Cell (PIC) method. Recent data obtained during operation of the eight Stationary Plasma Thrusters onboard the Express A#2 and A#3 Russian satellites are compared with computed values. Comparisons with induced moments measured during the firings are also presented.

Introduction

Since its conception over three decades ago the Hall thruster's[1,2] unique combination of high specific impulse and thrust-to-power ratio established it as a favored propulsion system for a variety of missions. In the former Soviet Union and more recently in Russia, over seventy Stationary Plasma Thrusters have been employed on spacecraft since the early seventies.[3] The October 1998 launch of the RHETT2/EPDM TAL (Thruster with Anode Layer) on the NRO STEx spacecraft also marked the first Western flight of a Hall thruster.[4] Employment of these thrusters continues to be evaluated, worldwide, for orbit insertion to LEO,[5] GEO station-keeping,[6] and in more ambitious missions for the human exploration and development of space.[7]

A critical engineering issue in the employment of these devices is the potentially hazardous interaction of their exhausts with spacecraft systems. Such interactions have unfavorable consequences on mission lifetime and, in some cases, may jeopardize mission success. Detailed evaluation and quantification of these effects, within the design of particular spacecraft, is a complex task with no comprehensive design tools or guidelines for the systems integrator in existence. Although numerous 2-D computer models for simulating Hall thruster plumes exist[8,9,10] most do not employ a Graphics User Interface (GUI) for easier use by the novice spacecraft designer. Also, due to the nature of the microscopic interactions in these plumes the numerical algorithms used are usually based on statistical particle techniques and require excessive computational resources. More importantly, the generated plume maps are of little use without a full 3-D interactions tool that allows the integrations engineer to quantify the spacecraft's response to plume impingement.

Science Applications International Corporation (SAIC) has developed a stand-alone suite of computer tools that permit the assessment of Hall thruster plume interactions with spacecraft systems. The components, all built for the Win32 platform, consist of (1) a fast, 1-D algorithm for determining conditions near the exit of Hall thrusters (to be used as input for 2-D plume simulations), (2) a 2-D plume code to map the thruster

[*] Presented as Paper IEPC-01-000 at the 27th International Electric Propulsion Conference, Pasadena, CA, 15-19 October, 2001.

[‡] Now with the Jet Propulsion Laboratory, Pasadena, CA.

plume in the R-Z plane, and (3) the Environment Work Bench (EWB), a 3-D plume-surface interactions code. The expertise to successfully carry out this effort is based on three decades of pioneering work during which the SAIC group (originally the Space Physics Group at Maxwell Technologies) developed spacecraft-environment interactions tools including NASCAP/GEO,[11,12] NASCAP/LEO,[13,14] POLAR,[15] DynaPAC,[16] and EPSAT.[17]

1-D Hall-Effect Thruster (HET) Algorithm

Algorithms used for simulating electric propulsion plumes assume that various conditions at the thruster exit are given. For example, the flow of expelled neutrals must be known before performing any calculations on charge-exchange ion production. In HETs several physical processes during operation have intrinsically different scale sizes for time and distance. It is therefore difficult to predict conditions at the exit using empirical observations exclusively. Furthermore, the effect of thruster geometry and operating conditions on the exhaust, and consequently the surrounding S/C surfaces, is difficult to assess by simple extrapolation of measured quantities from a given thruster.

A one-dimensional computer model of the Hall thruster has recently been developed at SAIC. [18] The model computes the electron current via the Generalized Ohm's law, which in the absence of the electromotive and thermoelectric terms is expressed as,

$$\frac{j_e}{n\,e\mu_e} = E + \frac{1}{n\,e}\frac{d\,p_e}{dx} \qquad (1)$$

where $\Omega_e \equiv \omega_B / \nu_m$ is the electron Hall parameter, with ω_B and ν_m being the electron cyclotron and momentum-exchange collision frequencies, respectively. The effective electron mobility coefficient, μ_e, in a direction perpendicular to the magnetic field is given by,

$$\mu_e = \frac{e}{m_e \nu_m}\frac{1}{1+\Omega^2} \qquad (2)$$

Collisions of electrons with neutrals, ions, and walls are accounted for through the total momentum transfer collision frequency:

$$\nu_m = \nu_{en} + \nu_{ei} + \nu_w \qquad (3)$$

where, ν_{en} and ν_{ei} are the electron-neutral and electron-ion collision frequencies, respectively. The primary mechanism that determines the effective wall collision frequency ν_w, is assumed to be that of secondary electron emission. The yield curve for secondary electrons as a function of impact energy has a universal shape with an almost linear rise at low energies. The Maxwellian average secondary yield is therefore assumed to vary according to,

$$\bar{Y} \equiv \frac{j_{e,s-w}}{j_{e,p-w}} \approx \frac{T_e}{E_1 / 2} \qquad (4)$$

where $j_{e,p-w}$ and $j_{e,s-w}$ are the primary and secondary electron current densities at the wall, respectively. E_1 is the secondary yield first cross over (taken as 50 eV for Boron Nitride). The model assumes that the yield does not exceed unity.

In steady state the electron fluid energy equation is given by,

$$\frac{\partial}{\partial x}\left(\frac{5}{2} j_e T_e + \kappa_e \frac{\partial T}{\partial x}\right) + E j_e = S \qquad (5)$$
$$S \equiv \boldsymbol{\varepsilon}_{\mathbf{ex}} + \boldsymbol{\varepsilon}_{\mathbf{i}} + \boldsymbol{\varepsilon}_{\mathbf{w}}$$

The first and second terms in the parentheses represent the energy density and heat fluxes, respectively with κ_e being the electron thermal conductivity perpendicular to the magnetic field. The electric power is denoted by the product Ej_e. The source term S on the right hand side accounts for electron energy losses due to e-n collisions that leave the neutral in an excited state (excitation) $\boldsymbol{\varepsilon}_{\mathbf{ex}}$, and those that eject the electron completely (ionization), $\boldsymbol{\varepsilon}_{\mathbf{i}}$. The wall loss term, $\boldsymbol{\varepsilon}_{\mathbf{w}}$, is obtained using the surface to volume ratio of the channel, the one-sided thermal flux, and the sheath potential.[18]

The numerical algorithm, written in Visual Basic, determines the evolution of particles based on the assumption that ions traverse each zone in a time scale that is much shorter than changes that occur in the electric potential. Therefore, the approach allows much faster convergence in comparison to other particle methods (min vs hrs).

Table 1. Comparison of SPT-100 computed and measured performance using the 1-D HET code.

Variable	Computed	Measured
I_d	3.7 A	4.5A
$\dot{m}_i / \dot{m}$	0.80	0.85-0.92
Thrust	90.2mN	83mN
Thrust eff.	0.6	0.5
Isp	1500sec	1600sec

Based on comparisons with recent Stationary Plasma Thruster (SPT-100) measurements the 1-D code has produced encouraging results. The acceleration channel in these simulations was augmented with an exhaust region (1cm-long) to capture plasma conditions near the exit plane. As shown in table 1, good agreement was achieved between measured and computed performance parameters (within 10-20%). The characteristic oscillatory behavior of the discharge current was also qualitatively captured (Figure 1).

2-D Plume Code

Second in the process of assessing plume interactions is the generation of the plume map. Once the required conditions at the thruster exit have been produced, by either the 1-D HET code described above or by other means (e.g. measurements), the plume map is generated using a 2-D, finite element (FE) code. The code has been developed by SAIC for the purpose of modeling electrostatic propulsion plumes, and has been applied with great success to ion thrusters[19] and Hall thrusters.[20] The tool incorporates a revised selection of computer modules from the 2-D, electrostatic code *Gilbert*. The algorithms are part of a general production tool for plume mapping that uses a Graphics User Interface (GUI). The GUI allows the user to specify easily the required parameter space for the engine under investigation and view the results graphically (Figure 2) on the same window.

The plume model consists of two main components: a Lagrangian algorithm for determining the expansion of the main beam and a Particle-in-Cell solver for computing ion production from charge-exchange.

Main Beam

The main beam is assumed to be comprised of a collisionless, singly-ionized, quasi-neutral plasma expanding in a density-gradient electric field. By comparison to heavy-particle motion, electrons reach dynamical equilibrium at much smaller characteristic times. The electron inertia term may therefore be neglected in the equation of motion:

$$m_e \frac{D\mathbf{v}_e}{Dt} = e\nabla\phi - \frac{\nabla p}{n} = 0 \qquad (6)$$

In equation (6), $\mathbf{v}_e$, ϕ and p are the electron velocity, electric potential and electron pressure, respectively. The electron mass is m_e and the charge is e. By assuming ideal gas behavior and isothermal electrons integration of equation (6) leads to the Boltzmann relation that can be expressed in terms of the electric potential,

$$\phi(n, T_e) = T_e \ln(n / n_\infty) \qquad (7)$$

with T_e being the electron temperature, n is the plasma density ($n=n_e=n_i$) and n_∞ is the reference plasma density at zero potential. Equation (7) is sometimes also known as the *barometric potential law*. In regards to the assumption of uniform electron temperature, measurements in the plume of various HETs suggest values that range between 6-11eV in the near-field region (where most of the charge-exchange events take place), falling to less than 2-3eV far from the thruster exit.[21,22,23] This suggests that a non-uniform temperature model which takes into account the effects of finite electron thermal conductivity would be more accurate. In light of the dominance of particle density gradients (and potential gradients) however, an isothermal model is assumed here. Unless otherwise stated, in all HET plume simulations mentioned here an effective temperature of 8eV has been used.

Ions are accelerated by the electric field, $E = -\nabla\phi$:

$$m_i \frac{D\mathbf{v}_i}{Dt} = -e\nabla\phi \qquad (8)$$

Since the drift velocity of the ions, **V**, is much greater than their thermal velocity, the high velocity ions are modeled as a fluid, **V**= $\mathbf{v}_i$). The steady state, conservation equations for mass and momentum (below) are solved in 2-D (R-Z) geometry.

$$\nabla \cdot n\mathbf{V} = 0$$
$$m_i \mathbf{V} \cdot \nabla \mathbf{V} = -\frac{\nabla p}{n} \qquad (9)$$

In comparison to PIC algorithms the Lagrangian modeling approach nearly eliminates the effects of numerical noise on the solution. Without incredibly fine zoning and large number of particles, PIC is also insufficiently accurate in the prediction of ion trajectories for problems with large-scale ratios (e.g. fractions of a millimeter to several meters). Finally, PIC requires considerably longer computational times (e.g. minutes of real time on an 800MHz PC versus tens of hours of CPU time on parallel IBM SP/SP2 processors).[8]

Neutral Gas Density

The neutral gas density has two components in space: un-ionized (beam) particles from the thruster and un-ionized particles from the hollow cathode. The beam of neutrals from the thruster is computed using an annular anode gas flow model with isotropic emission from a ring. The profile of neutrals from the thruster is computed using two disk emissions defined by angles $\Omega(r_o,r,z)$ and $\Omega(r_i,r,z)$ for the outer and inner thruster radii, respectively,[20] and subtracting the smaller from the larger:

$$n_{HET}(r,z)=\frac{2F_o\left(\Omega(r_o,r,z)-\Omega(r_i,r,z)\right)}{m_i u_o \pi\left(r_o{}^2-r_i{}^2\right)} \qquad (10)$$

where, F_0 is the neutral flow rate, u_0 is the neutral speed at the thruster exit and m_i is the particle mass. The inner and outer radii of the acceleration channel are denoted by r_i and r_o, respectively.

The hollow cathode is offset by a distance r_{HC} from the thruster. The constant-temperature neutrals are emitted isotropically from the neutralizer. Their distribution $n_{HC}(z)$ is estimated based on,

$$n_{HC}(z)=\frac{F_{o,HC}}{\pi m_i u_{o,HC}}\frac{z}{(\max[r_{HC},r]^2+z^2)^{3/2}} \qquad (11)$$

where, $F_{o,HC}$ is the mass flow rate and $u_{o,HC}$ is the particle speed.

For simulation of plumes in the laboratory, a third contribution to the neutrals is added based on the chamber background density, and is assumed to be uniform.

Neutral-Ion Interactions

Fast ions from the main beam undergo charge-exchange (CEX) with neutral particles, resulting in slow-moving ions and fast-moving neutrals,

$$_{fast}Xe^+ + {}_{slow}Xe \rightarrow {}_{slow}Xe^+ + {}_{fast}Xe \qquad (12)$$

CEX is computed using a two-dimensional PIC code. The main beam ion densities computed by the Lagrangian calculations, and the neutral gas profile (above), are the input for the calculation. The rate of CEX-ion production, n_{CEX} is determined by,

$$n_{CEX}=n\mathbf{V}\sigma_{CEX}n_o \qquad (13)$$

where, n_o is the neutral particle density and σ_{CEX} is the resonant CEX collision cross section. In all ensuing comparisons with computed values (using Xenon) a constant value has been assumed (~55 Å^2).[24] The CEX-ion density is computed by tracking particle trajectories in density-gradient electric fields using a finite-current barometric law for the electron density (electron current equals ion current). The code solves Poisson's equation on a finite element grid and iterates until steady state CEX densities and potentials are self-consistent. A model to correctly account for elastic collisions of ions with neutrals at small impact parameters has also been recently included.[20]

Recent Modeling and Comparisons

In the past few years the 2-D plume code has been applied successfully in a variety of electrostatic propulsion plume simulations. Modeling of the Deep Space 1 (DS-1) ion thruster plume showed reduced charge-exchange (CEX) ion concentrations in space compared to the laboratory, confirming the enhancing effect of vacuum chamber neutrals on CEX ion production.[19] Simulations of 4 kW Hall thruster plumes provided critical insight into ion-neutral collision processes that occur in the laboratory. Guided by empirical observations these calculations exposed neutral-ion processes, not previously modeled, that produce highly energetic ions (>100V) at large angles (in addition to the low-energy CEX ions expected to be present there).[20] In certain cases these ions can be the dominant high-energy particles at large angles relative to the thrust direction, and may therefore contribute substantially to the sputtering of spacecraft surfaces.

More recently, comparisons with data (courtesy of the NASA Glenn Research Center)[25,26] acquired from two Russian geosynchronus communication satellites, Express A#2 and A#3, yielded good agreement with values computed by the 2-D plume code. Both spacecraft were launched aboard Proton launch vehicles from the Baikonur Cosmodrome in Kazakhstan. Express-A #2 was launched on March 12, 2000 and is currently in orbit providing telecommunication services for Russian television and network operations. Express-A #3 was launched on June 24, 2000 to replace the (aging) Statsionar-11 (Gorizont-26). It is used for high-speed Internet access to the Middle East and Africa from Europe. Both satellites employ eight, Stationary Plasma Thrusters (SPT-100) for station-keeping. The comparisons between measurements and plume simulations are described in greater detail below.

EXPRESS-A #2

Measurements from two ion-flux sensors ("DRT") and three electric field sensors ("DEP") onboard the Russian Express-A #2 spacecraft were provided. Data from one ion-flux sensor was used, the DRT1. The second sensor is positioned under the MLI and did not provide useful information. The position of DRT1 and thruster unit #4 (TU4) on the A #2 spacecraft are shown in Figure 3. The unit consists of two SPT100s: the T4 (left) and RT4 (right). The DRT1 sensor is at a distance of 1.352m from RT4, at an angle of approximately 80deg relative to the Xc axis. Signals during this thruster's operation have been used for comparisons.

Two different simulation cases of plume maps were initially performed for the A #2 satellite, distinguished by two mass flow rate values: 4.9 and 5.3 mg/s for the thruster and 0.49 mg/s and 0.371mg/s, respectively, for the cathode-neutralizer. Results from the higher mass flow rate case are presented here. The generated plume maps (and trajectories) are graphically illustrated in Figure 2.

The plume model computes the ion current density at the position of the DRT1 detector to be 19.9mA/m^2 for the low flow-rate case (4.9mg/s), and 26.9mA/m^2 for the higher flow-rate (5.3 mg/s). The DRT1 signals indicate significant fluctuations, 16-41 mA/m^2, during a 2-hour operation of RT4 on 4/13/200 (Figure 4, top). Data from momentary firings of the same thruster on different dates also show noticeable variations. The sensors registered values that ranged between 13-25mA/m^2 (Figure 4, middle) on 3/16/2000 and 18-52 mA/m^2 on 5/5/2000 (Figure 4, bottom). Signals from the T4 thruster during continuous operation on 4/12/2000 were characterized by reduced fluctuations with an average value of about 13mA/m^2. According to Russian engineers, the large ion-flux variation during the operation of RT4 may be due to *burning of thruster material* commonly taking place during the first firings of these thrusters.[27] This would indeed alter the effective mass flow rate during operation and therefore the observed ion flux.

EXPRESS-A #3

Data from the Express-A #3 spacecraft was also provided. The measurements were registered by two ion-flux sensors (DRT1 and DRT2) located at the sides of the (rotating) solar arrays (Figure 5). DRT3-1, the sensor located at the same position as the DRT1 in the A #2 satellite, registered zero values. Contrary to the A #2 satellite the second sensor, DRT3-2, (positioned under the MLI) provided non-zero readings. These could not be compared to (2-D) computed values however due to the orientation of the sensor relative to the thruster (upward) and possible interference by other S/C structures.

Results from the Express-A #3 simulations and comparisons with measurements are presented in Figure 6 through Figure 8. As in the A#2 calculations, a mass flow rate of 5.3 mg/s for the thruster and 0.371mg/s for the cathode-neutralizer were used as input values to the model. A map of the main beam expansion (used for comparison with data from the DRT sensors on the solar arrays) is shown in Figure 2 (top, right). The plume model computes an ion current density at the position of the DRT1 detector (3.542m away) of 41.6 μA/cm^2 at 0 deg (wrt the axis of symmetry) and 35 μA/cm^2 at 10 deg. During three different RT4 firings the values measured by the sensor - when the solar array angle was at 0 deg wrt to Xc axis - varied from 36 to 54 μA/cm^2 (Figure 6). Additional comparisons with values registered by the DRT2 sensor are presented in Figure 7. The measurements were taken during operation of the RT3 SPT100. The energy spectra in Figure 8 suggest a high-energy peak of between (E/q=) 233.3-247.1 V at

this location. The computed value is (E/q=) 229 and 234 V for plume angles of 0 and 10 deg, respectively.

All (useful) ion-flux measurements from both spacecraft, taken at various times during the acquisition period and at different locations with respect to the center of gravity, were compiled and scaled (~$1/r^2$) down to a 1-m radius.[27] Figure 9 shows a comparison between these measurements and computed values as a function of plume angle. As alluded to earlier, although the precise nominal mass flow rate during operation of the thrusters is not known, computed values were produced using 5.3 mg/s of anode flow rate. The comparison suggests that the model over predicts the mean measured value by approximately 20% for angles less than 20 deg. The effective electron temperature however during operation is unclear. The value of 8eV used here may have been higher. For comparison purposes Figure 9 also shows computed values for a (uniform) electron temperature of 11eV. In regards to the values at the larger angles, the comparison is inconclusive due to the large spread in the data.

3-D Environment Work Bench (EWB)

Plume interactions with spacecraft subsystems, in three dimensions, are determined with the Environment Work Bench (EWB). For Hall (and ion) thrusters the maps produced with the 2-D plume tool are used as input.[§] Existing models that are relevant to interactions with electric propulsion plumes are described below.

Fluxes to Surfaces and Sputtering

The thruster ion flux at any point, i, on a surface j, due to plume component k, is calculated as follows:

$$F_{ik} = \rho_{ik}\left|\vec{u}_{ik}\right|\cos(\theta_{ik}), \quad \cos(\theta_{ik}) = \frac{\vec{n}_j \cdot \vec{u}_{ik}}{\left|\vec{n}_j\right|\left|\vec{u}_{ik}\right|} \qquad (14)$$

In equation (14), ρ_{ik} is the ion particle density and $\vec{u}_{ik}$ is the ion velocity. The angle between the surface normal vector $\vec{n}_j$, and the particle velocity is denoted by θ_{ik}. Fluxes to points on surfaces account for the interference ("blocking") by other spacecraft surfaces. Specifically, if a straight line between the point in question and the thruster orifice intercepts any other surface the flux is zero.

The sputtering of a spacecraft surface j at point i, due to energetic ion impact from the thruster is calculated based upon the material sputtering rate, $R_{ij}{}^{S}$:

$$R_{ij}{}^{S} = \sum_k Y_{ijk} F_{ik}, \quad Y_{ijk} = Y_{ijk}(E_{ik}, \theta_{ik}) \qquad (15)$$

where, Y_{ijk} is the sputter yield of the material on surface j. The sputter yield depends on the material, the energy of the ions impacting the surface and the angle between the flux vector and the surface-normal. All formulae are polynomial fits to sputtering measurements and can therefore be easily updated with improved models.

Surface Erosion and Deposition

An example of calculated sputtered erosion depth and redeposition thickness on a typical communications satellite is shown in Figure 10. Depending upon the duration of thruster operation, t, the total surface erosion by direct plume impact, as well as re-deposition of sputtered particles onto other surfaces, is determined by computing a net erosion/deposition rate. The net rate is calculated as follows: for each spacecraft structure j the sputtering rates at all points are averaged to produce a source term $R_j{}^{S}$, at the centroid of that surface. This source term is then used to calculate a deposition rate at each of the grid points for all surfaces:

$$R_i{}^{D} = (1/2\pi)\sum_j R_j{}^{S}\Omega_{ij}\cos(\Theta) \qquad (16)$$

where, Ω_{ij} is the solid angle subtended by surface j at point i, and Θ is the angle between the normal of the depositing surface and a ray from the sputtered surface centroid to point i. The net rate, R_i is then computed at each point by,

$$R_i = R_i{}^{D} - R_i{}^{S} \qquad (17)$$

If $R_i > 0$ it is a deposition rate, if $R_i < 0$, it is an erosion rate. This rate is then integrated over the mission duration to get a total number of deposited particles per square meter. The integrated value is determined by calculating an average rate and then

[§] Plume maps generated using different simulation tools, such as Direct Simulation Monte Carlo (DSMC) or Magnetohydrodynamic (MHD) codes, may also be easily incorporated in EWB.

multiplied by the mission duration. This accounts for time-dependent changes in spacecraft geometry (such as solar array rotation).

Hall and ion thruster plume maps have been recently incorporated in EWB for the purpose of gaining detailed guidance towards the design of a direct-drive Hall thruster system.[28] Figure 12 shows the simulated exhaust ion densities from an SPT100 onboard the EWB-generated Express-A spacecraft model. Figure 13 depicts ion densities from the DS-1, 30-cm ion thruster.

Surface Heating

The incident heat flux at each point on a spacecraft surface, Q_i, due to plume impact is calculated as follows:

$$Q_i = \sum_k K_\perp F_{ik} E_{ik\perp} + K_\parallel F_{ik}\ E_{ik\parallel} + F_{ik}\left(e\phi_{ionize}\right)$$
$$E_{ik\perp} = \frac{1}{2} m u_{ik\perp_i}^2 \quad E_{ik\parallel} = \frac{1}{2} m u_{ik\parallel_i}^2 \tag{18}$$

where, m is the (propellant) ion mass. $K_\perp$ and $K_\parallel$ denote perpendicular and parallel accommodation coefficients, respectively. These are material-dependent coefficients relating incident to reflected quantities. The ionization energy is given by ϕ_{ionize}. An example of calculated heating rates on a typical communications satellite is shown in Figure 11.

Forces and Induced Torques

The model for determining the induced torque Γ on the spacecraft during thruster operation accounts for contributions from the thrust and from exhaust impingement on surfaces:

$$\Gamma = \sum_T \Delta r_T \times (-f_T) + \sum_j \Delta r_j \times f_j \tag{19}$$

where, $\Delta r = r - r_0$ is the position vector of surface j or thruster T form a reference point with position vector, r_0. The force f_j is the momentum imparted to a surface from plume particles, per unit time. A choice to use either *specular* elastic reflection from the surface (colliding particle is reflected with the same speed and incidence angle equals the reflection angle), or diffuse reflection (based on material-dependent accommodation coefficients), is available. For example, in the case of *specular* reflection the momentum imparted normal to the surface per particle collision is:

$$M_n = m(u_{inc} \bullet n - u_{ref} \bullet n) = 2m\left|u_{inc} \bullet n\right| \tag{20}$$

Where u_{inc} and u_{ref} are the incident and reflected particle velocities, respectively. The incremental (normal) force, df_n on an element of surface area dA, due to incident particle flow $\rho m(u_{inc} \bullet dA)$, is given by

$$df_n = M_n \rho m(u_{inc} \bullet n)\, dA = 2\rho m(u_{inc} \bullet n)^2 dA \tag{21}$$

Figure 14 illustrates computed torques, induced by the Express-A SPT100's, as a function of solar array angle (see Figure 5). A specular solar array surface was assumed for these calculations even though the Express-A reports suggest that the back and front surfaces may have different reflective properties. Additional information would be required (e.g. material-specific momentum accommodation coefficients) for the case of a diffusive reflective surface. Comparisons with measured values as a function of solar array angle suggest good qualitative agreement. A number of issues regarding the way and time this data was obtained are still under investigation. The oscillation asymmetry induced by the high torque values at 240deg SA angle, suggest that the back and front surfaces of the array may indeed have distinct reflective properties. This has not yet been confirmed for the Express-A spacecraft. Also, the relatively high values at 0deg and 180deg for the My and Mz moments are questionable. All data continue to be reviewed.

Conclusions

A comprehensive computer package has been presented for modeling Hall thruster plume interactions with spacecraft systems. The PC-based tool is a suit of easy-to-use computer codes that allow the systems integration engineer to assess interactions of a given thruster and/or perform test cases for different geometries and operating conditions. Typically, 3-D interactions analyses can be performed only after the required parameter space, such as thruster exit conditions and plume map, have been provided. Most often such information is supplied by independent sources, for a given thruster, and does not offer the luxury of assessing interactions under

varying operating conditions. The stand-alone, HET interactions package allows the user to conduct the complete interactions cycle: estimate thruster conditions, generate the plume map and determine the 3-D effects on S/C surfaces for different configurations and conditions. All three major components of the computer tool have been applied successfully to a variety of problems related to electrostatic propulsion. Most recently, the first flight data on Stationary Plasma Thrusters have been obtained from the Russian Express-A satellite, and have been compared with 2-D plume simulations. The comparisons yield good agreement with ion flux measurements for the main beam. The computed values are also within the large spread measured at the larger angles where most of the charge-exchange ions are concentrated. Induced torque calculations with EWB also produced good qualitative agreement with the measurements.

Acknowledgments

We are grateful to David Manzella, Todd Peterson and Robert Jankovsky of the NASA Glenn Research Center for providing us with the Express/SPT100 reports and data.

References

[1] Haines, M.G., "The Acceleration of a Plasma by an Electric Field Using the Hall Effect," International Conference of Ionization Phenomena in Gases, Paris, 1963.

[2] Morozov, A.I., et al., "Plasma Acceleration with Closed Electron Drift and Extended Acceleration Zone," *Sov. Phys. Tech. Phys*., Vol. 17, No. 38, 1972.

[3] Bober, A.S. and Maslennikov, "SPT in Russia – New Achievements," Proceedings of the 24th International Electric Propulsion Conference, Sep. 1995, pp. 54-60.

[4] Naval Research Laboratory, "Naval Research Laboratory Goes Operational With United States First Hall Thruster Electric Propulsion System," Press Release, Oct. 29, 1998.

[5] Oleson, S.R., "Electric Propulsion for Low Earth Orbit Communications Satellites," IEPC paper 97-102, Aug. 1997.

[6] Oleson, S.R., Myers, R.M., "Advanced Propulsion for Geostationary Orbit Insertion and North-South Station Keeping," *Journal of Spacecraft and Rockets*, Vol. 34, No. 1, pp. 22-28, Jan-Feb 1997.

[7] Oleson, S.R. and Sankovic, J.M., "Advanced Hall Electric Propulsion for Future In-Space Transportation," NASA TM-2001-210676.

[8] VanGilder, D.B., Boyd, I.D., and Keidar, M., "Particle Simulations of a Hall Thruster Plume," *Journal of Spacecraft and Rockets*, Vol. 37, No. 1, 2000, pp. 129-136.

[9] Oh, D. and Hastings, D., "Experimental Verification of a PIC-DSMC Model for Hall Thruster Plumes," Paper AIAA-96-3196, Lake Buena Vista, FL, 1996.

[10] Samanta Roy, R.I., Hastings, D.E., and Gatsonis, N.A., "Numerical Study of Spacecraft Contamination and Interactions by Ion-Thruster Effluents," *Journal of Spacecraft and Rockets*, Vol. 33, No. 4, 1996, pp. 535-542.

[11] Mandell, M.J., P.R. Stannard, and I. Katz, NASCAP Programmer's Reference Manual, S-Cubed Division of Maxwell Laboratories, 1984.

[12] Rubin, A. G., I. Katz, M. J. Mandell, G. Schnuelle, P. Steen, D. Parks, J. J. Cassidy, and J. C. Roche, "A Three-Dimensional Spacecraft-Charging Computer Code," in H.B. Garrett and C.P. Pike, ed., Space Systems and Their Interactions with Earth's Space Environment, *Progress in Astronautics and Aeronautics*, Vol. 71, AIAA 1980.

[13] Mandell, M.J. and I. Katz, "High Voltage Plasma Interactions Calculations Using NASCAP/LEO," AIAA Paper 90-0725, 1990.

[14] Mandell, M.J., I. Katz, V.A. Davis, and R. A. Kuharski, "NASCAP/LEO Calculations of Current Collection," in *Current Collection From Space Plasmas*, NASA CP3089, 1990.

[15] Murphy, G. and I. Katz, "The POLAR Code Wake Model: Comparison with in situ observations, *Journal of Geophysical Research*, Vol. 94, 9065, 1989.

[16] Mandell, M.J., T. Luu, J. Lilley, G. Jongeward, and I. Katz, “Analysis of Dynamical Plasma Interactions with High Voltage Spacecraft,” (2 volumes), Rep. PL-TR-92-2258, Phillips Lab., Hanscom Air Force Base, MA, June 1992.

[17] Jongeward, G.A., R.A. Kuharski, E.M. Kennedy, K.G. Wilcox, N.J. Stevens, R.M. Putnam, and J.C. Roche, “The Environment Power System Analysis Tool Development Program," in *Current Collection From Space Plasmas*, NASA CP3089, 1990.

[18] Mikellides, I.G., *et al*., “A 1-D Model of the Hall-Effect Thruster with an Exhaust Region,” AIAA Paper 2001-3505, July 2001.

[19] Davis, V.A., *et al*., “Ion Engine Generated Charge Exchange Environment: Comparison Between NSTAR Flight Data and Numerical Simulations,” AIAA Paper 00-3529, July 2000.

[20] Katz, I., *et al*., "A Hall Effect Thruster Plume Model Including Large-Angle Elastic Scattering," AIAA Paper 01-3355, July 2000.

[21] Kim, S. W., Foster, J. E., and Gallimore, A. D., "Very-Near-Field Plume Study of a 1.35 kW SPT-100," AIAA Paper 96-2972, July 1996.

[22] Fife, J.M., “Hybrid PIC-Modeling and Electrostatic Probe Survey of Hall Thrusters,” Ph.D. Dissertation, 1998, Massachusetts Institute of Technology, Massachusetts.

[23] Haas, J.M., and Gallimore, A.D., “An Investigation of Internal Ion Number Density and Electron Temperature Profiles in a Laboratory-Model Hall Thruster,” AIAA Paper 00-3422, July 2000.

[24] Pullins, S., Dressler, R.A., Chiu, Y., and Levandier, D.J., "Ion Dynamics in Hall Effect and Ion Thrusters: Xe^{+} + Xe Symmetric Charge Transfer," AIAA Paper 00-0603, January, 2000.

[25] Task 27A Completion Report, NASA Contract NAS3-99151, SPI Subcontract 97-1088-02, “Acquire TM Data for Type A and Type B Sensors for Express-A No3 Satellite (Period of 24 June 2000 to and including 30 September 2000),” NPO PM-Razvitie, 2001.

[26] Task 27B Completion Report, NASA Contract NAS3-99151, SPI Subcontract 97-1088-02, “Acquire TM Data for Type A and Type B Sensors for Express-A No3 Satellite (Period of 01 October 2000 to and including 31 December 2000),” NPO PM-Razvitie, 2001.

[27] David Manzella, *et al*., “Hall Thruster Plume Measurements On-board the Russian Express Satellites” IEPC Paper, 2001-44, Oct. 2001.

[28] Jongeward, G.A., Mikellides, I.G, and Katz, I., “High Voltage Solar Arrays for a Direct Drive Hall Effect Propulsion System,” IEPC Paper 2001-327, Oct. 2001.

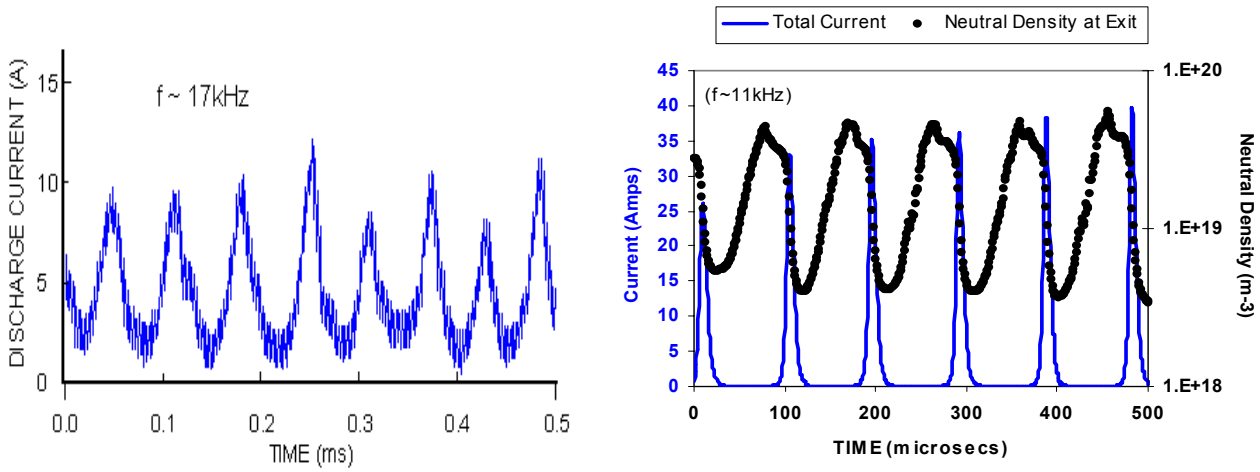

Figure 1. Left: Measured evolution of the discharge current for the SPT-100 (data taken during tests at NASA/GRC).Right: Computed evolution of the discharge current and neutral density (at exit) using the 1-D, Hall thruster computer model.

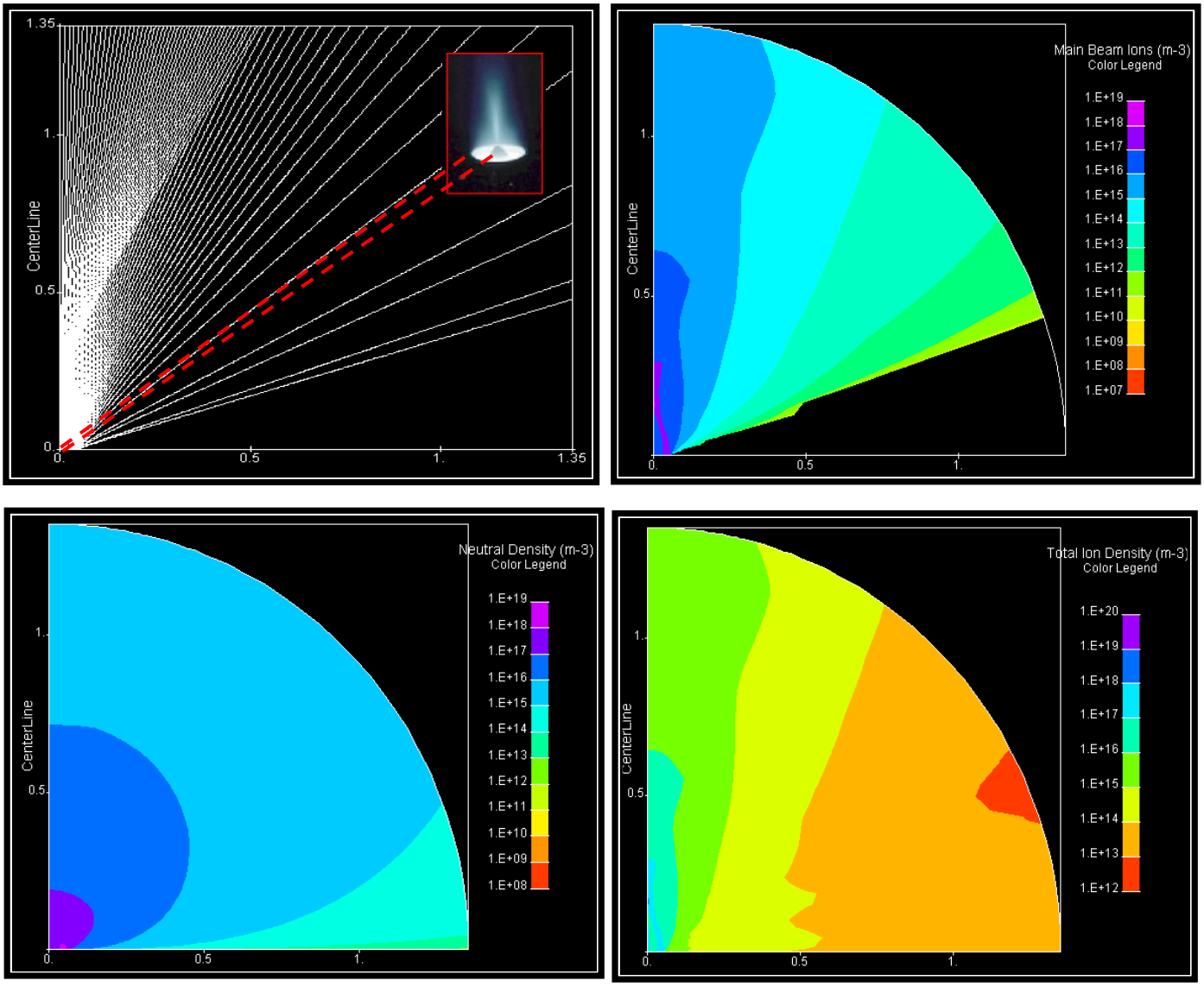

Figure 2. Results of 2-D plume simulation of SPT100 showing ion trajectories (top left), main-beam ion density (top right), neutral density (bottom left) and total ion density (bottom right).

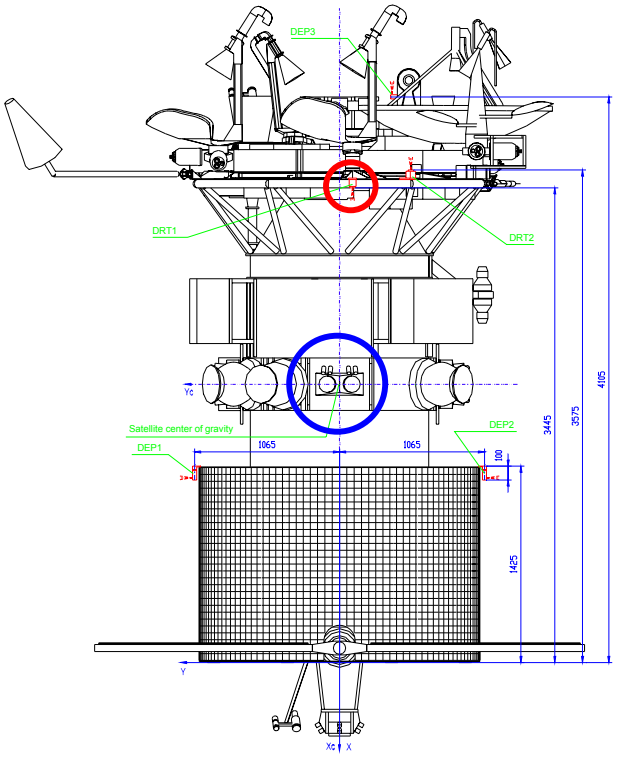

Figure 3. Side view of the Express A#2 spacecraft. Circled are the ion flux sensor (small circle) and SPT100 unit (large circle).

SPT100 Unit

RPA Sensor

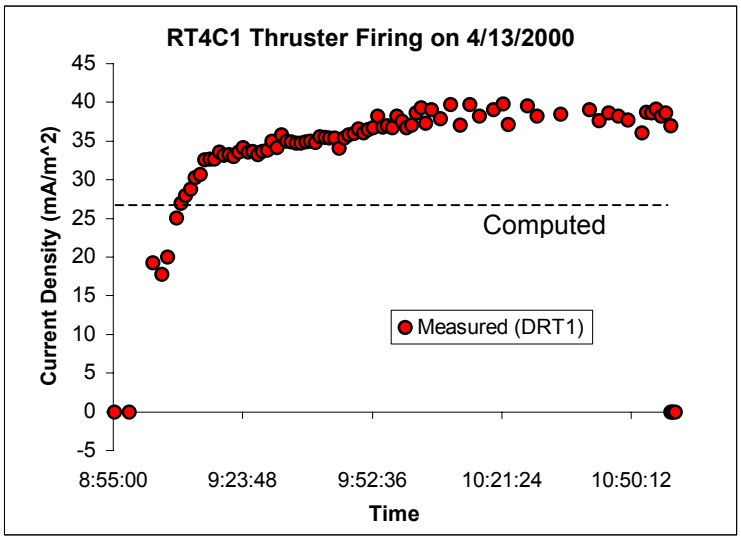

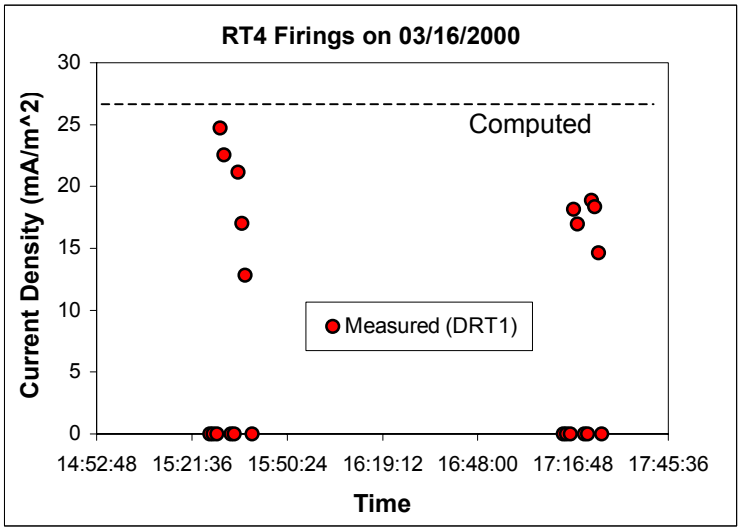

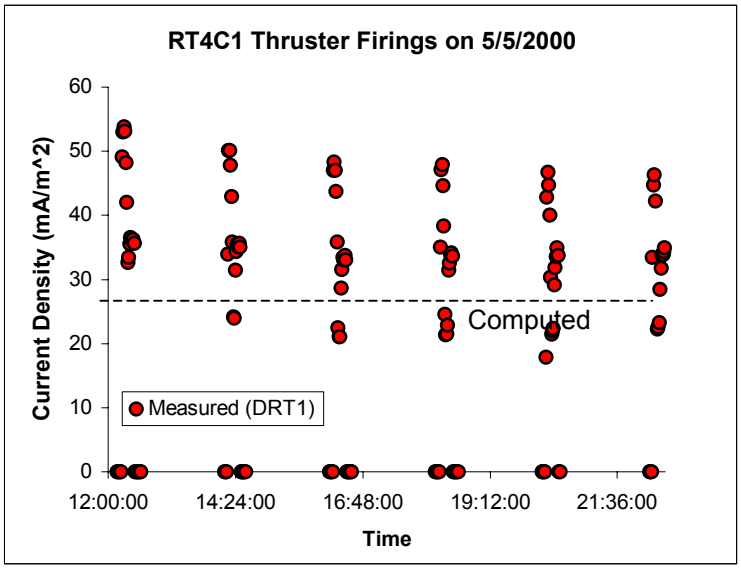

Figure 4. Comparison between computed and measured current densities as registered onboard the Russian Express A#2 spacecraft.

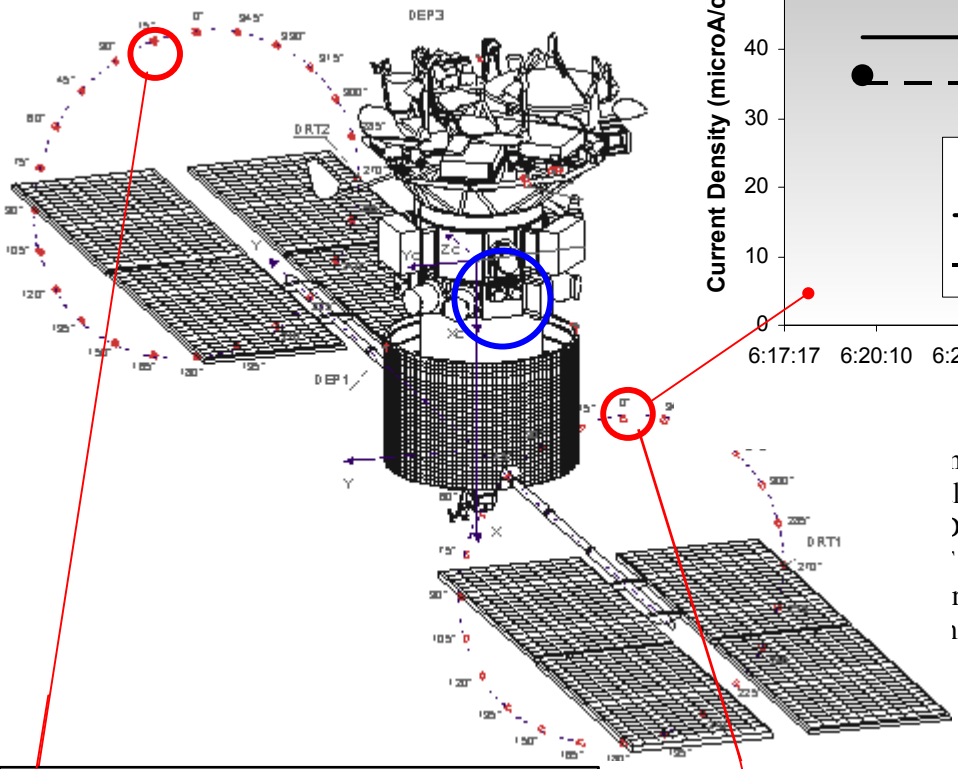

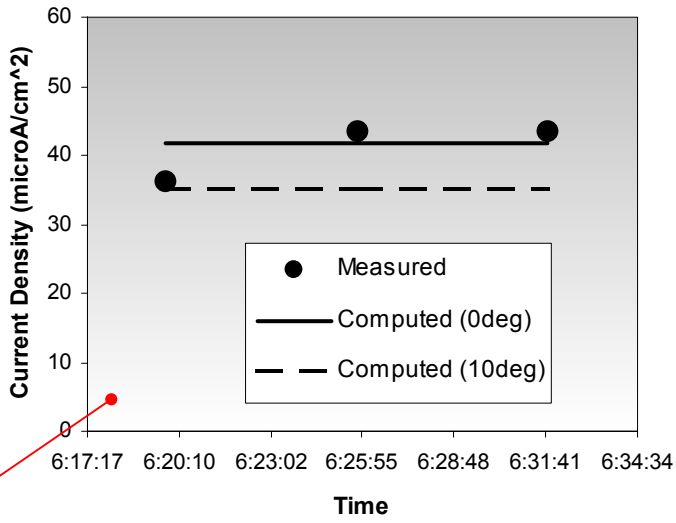

mparison between computed and lues onboard the Express A#3 Data obtained during firings of '100 on 6/7/2000. The DRT1 roximately 3.8 m away from the ı the SA angle is 0 deg.

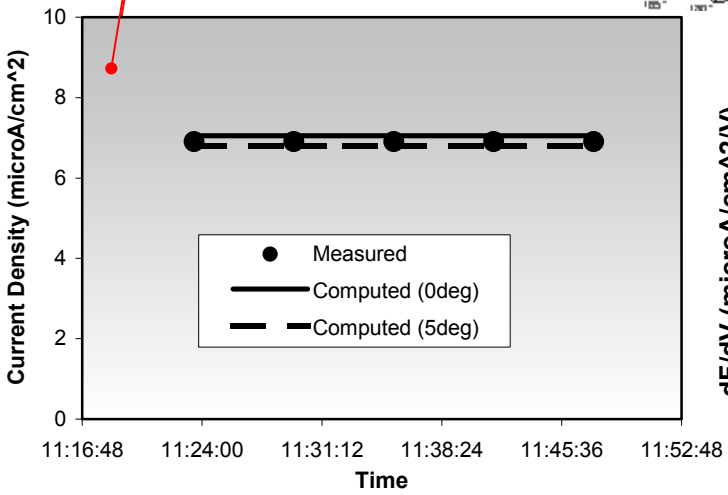

Figure 7. Comparison between computed and measured values onboard the Express A#3 spacecraft. Data obtained during firings of the RT3 SPT100 on 7/9/2000. The DRT2 sensor is approximately 8.76 m away from the thruster when the SA angle is 15 deg.

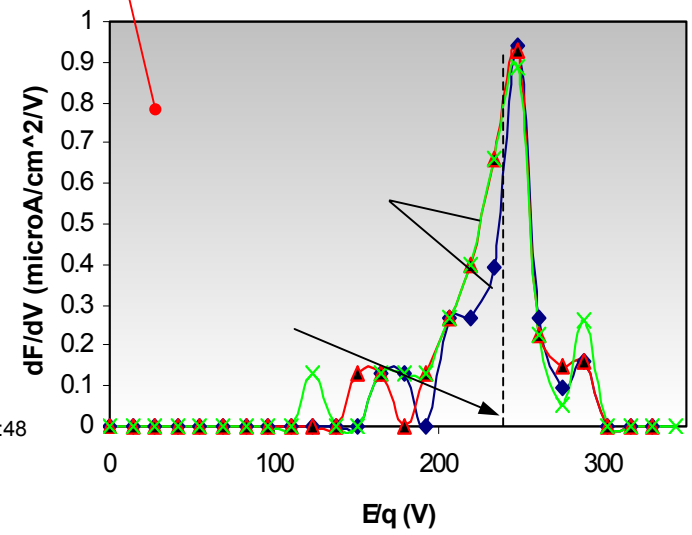

Figure 8. Computed value of the main beam ion energy and measured energy spectra onboard the Express A#3 spacecraft. RPA values obtained during firings of the T4 SPT100 on 6/7/2000.

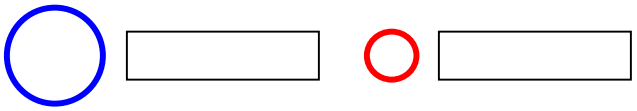

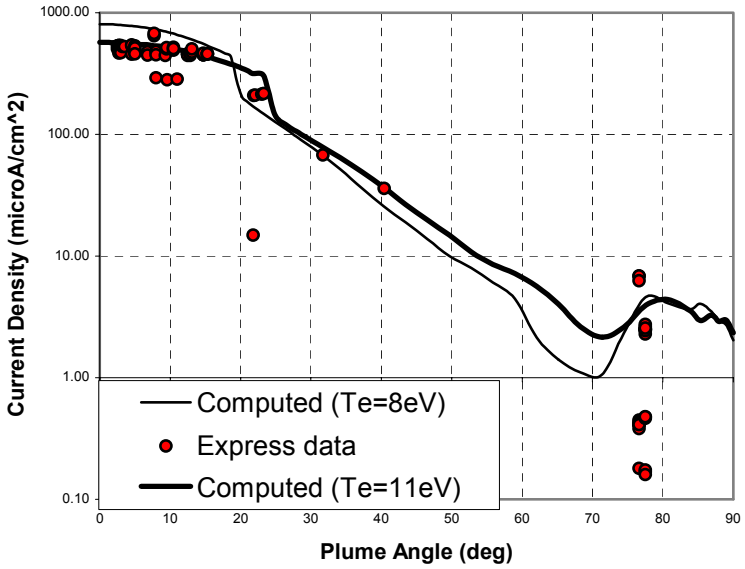

Figure 9. Comparison between current density measurements on board the Express-A spacecraft and computed values using the 2-D plume code at a radius of 1 m. Measurements taken at different locations were scaled down to 1-m using a $1/r^2$ scaling.

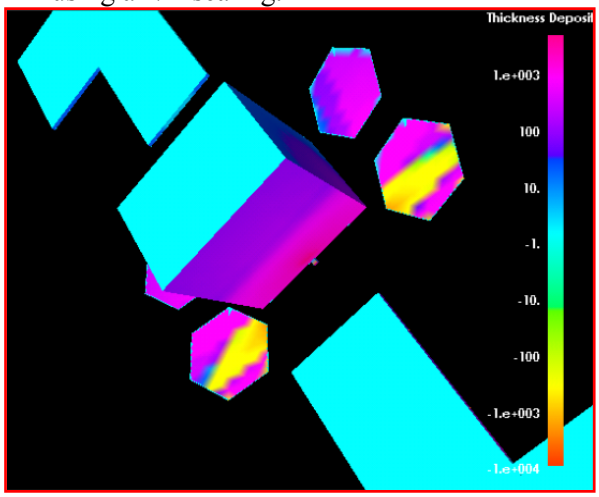

Figure 10. Sputtered erosion depth and redeposition thickness on typical satellite.

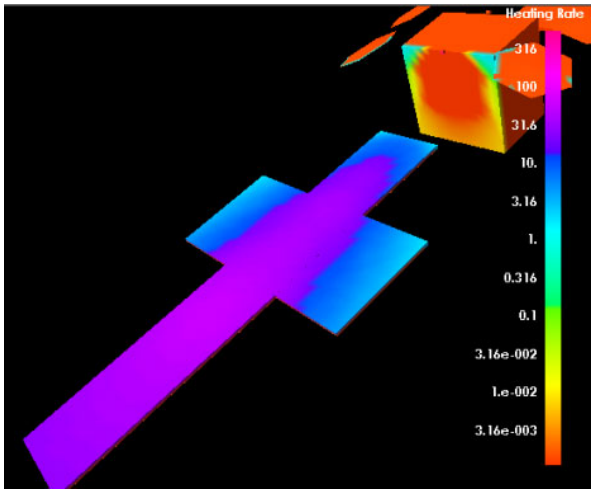

Figure 11. Surface heating due to thruster plume impingement and ionization.

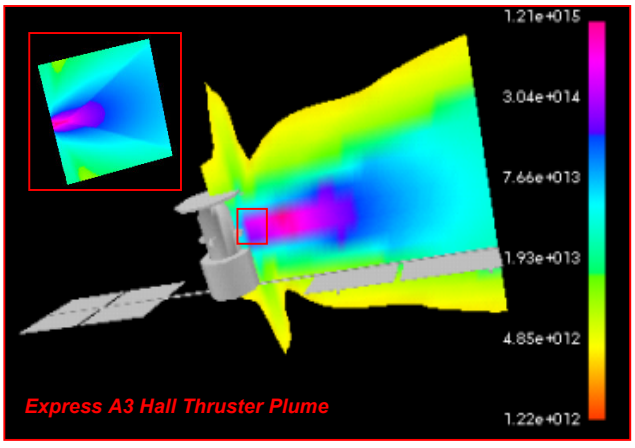

Figure 12. Ion particle density (in m^{-3}) from an SPT100. The spacecraft is the EWB-generated model of the Express satellite.

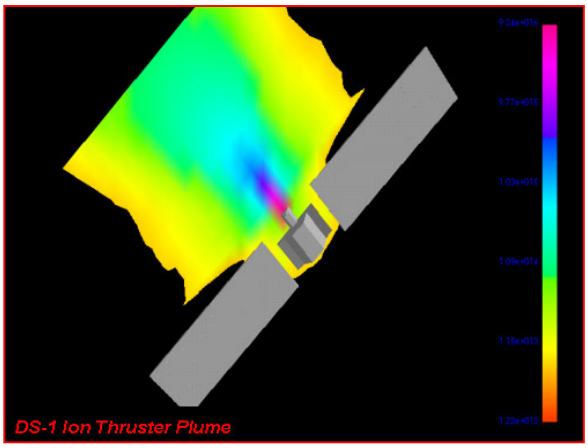

Figure 13. Ion particle density (in m^{-3}) from a 30-cm ion thruster. The spacecraft is the EWB-generated model of DS-1.

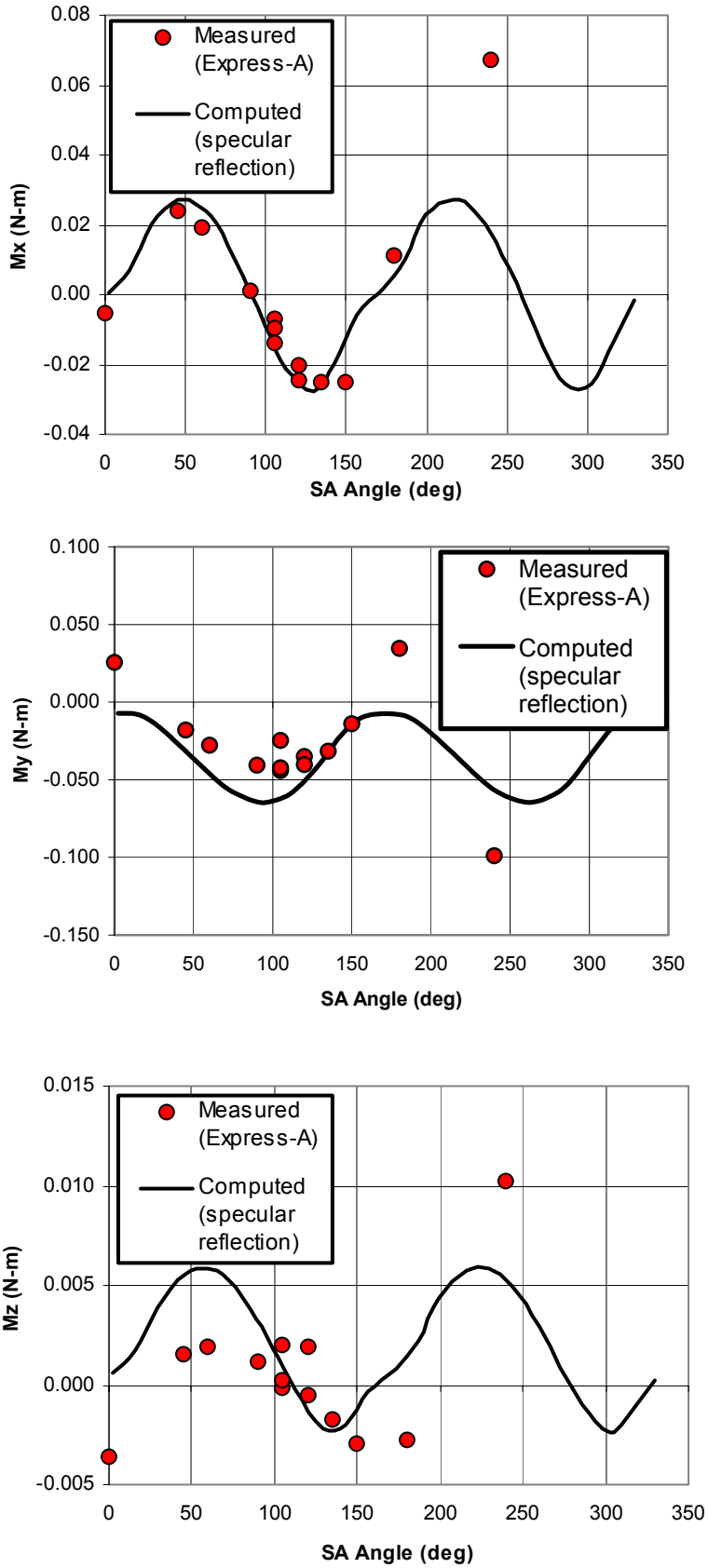

Figure 14. Comparison between computed and measured torques induced by firings of the RT4 SPT100 onboard the Express-A spacecraft. The data was acquired during a rotation of the solar array.